Annals of Biomedical Engineering, Vol. 30, pp. 1152–1161, 2002
Printed in the USA.

0090-6964/2002/30(9)/1152/10/$15.00

Thermal Model for Fast Simulation During Magnetic Resonance Imaging Guidance of Radio Frequency Tumor Ablation

PETER C. JOHNSON and GERALD M. SAIDEL

Department of Biomedical Engineering, Case Western Reserve University, Cleveland, OH

(Received 26 July 2001; accepted 20 August 2002)

Abstract—Thermal ablation of a tumor with radio frequency (rf) energy from a small probe inserted into the solid tumor can be accomplished with minimal invasiveness under guidance with magnetic resonance imaging (MRI). A theoretical study is presented of 3D temperature distribution dynamics in tissue with rf heating to show the feasibility of fast numerical solution for repeated simulations during an ablation procedure. Model simulations are intended to be used during an ablation treatment together with temperature field images obtained by MR to predict the effect of alternative strategies of source heating and placement. A feature of the model is that it incorporates a heat source term that varies with distance from the rf probe to avoid the need for solving electric field equations. The effects of perfusion and internal cooling of the rf probe on the temperature distribution are simulated to show the model flexibility. Using a personal computer (PC), numerical solution of the model equations required 10 s to 2 min depending on the perfusion–temperature relationship. The results show the feasibility of using thermal model simulations in an iterative manner with MR images to help guide thermal ablation procedures in the clinical setting. © *2002 Biomedical Engineering Society.* [DOI: 10.1114/1.1519263]

Keywords—Radio frequency ablation, Thermal model, Coagulative necrosis, Bioheat equation, Modeling, Interventional MRI.

INTRODUCTION

Thermal ablation (a.k.a. coagulative necrosis) of a tumor using radio frequency (rf) energy from a small probe can be accomplished with minimal invasiveness under guidance with magnetic resonance imaging (MRI).[11] From an electrode at the probe tip, an alternating electric current passes through the tissue to cause heating that can lead to cell death and apoptosis depending on the temperature and duration of heating.[15,22] MR systems can assist in inserting and positioning the rf probe, monitoring the thermal therapy, and evaluating the procedure results. Ablation monitoring by MR provides temperature maps in addition to anatomical tissue-contrast images. These temperature maps acquired repeatedly during the procedure can assist the clinician in maximizing tumor destruction and minimizing damage to the surrounding normal tissue. Characteristics of MRI have been used to examine the tissue temperature distribution produced by the rf heat source using low field strength magnets.[5,20]

Currently, procedural decisions with respect to sequential positioning the probe and the conditions of the rf energy input rely solely on the experience of the clinician in interpreting the MRI data. If, in addition to MR images, model simulations were available to the clinician to predict tissue temperature and ablated regions with little or no perfusion during a procedure, then the effectiveness and reliability of this interventional treatment could be improved. Such improvement requires that model simulations of 3D tissue temperature dynamics be accomplished many times during the procedure. To make this clinically feasible, each model simulation should be accomplished in the order of seconds using a personal computer (PC). The main objective of this study is to show that fast simulations are feasible with a novel model and a combination of well-established and efficient numerical methods.

A typical rf ablation procedure involves inserting the MR-compatible rf probe into the desired location within a tumor under near real-time MR guidance. For interstitial thermal ablation, the rf power input is sustained between 6 and 40 min depending on the desired lesion volume.[13] The duration of the ablation heating in a probe position is based on estimates of the time required to reach an approximate thermal steady state. This may be significantly longer than necessary to produce the optimal damage. A better determination of the optimal duration can be achieved by a model that can quantitatively evaluate thermal damage with time at any point in the tumor. With respect to the target tissues of interest for this study as well as clinical preference, we will consider ablations that take about 10 min. During an ablation procedure, a sequence of heating and imaging might consist of successive periods of heating for 15 s followed by

Address correspondence to Gerald M. Saidel, Ph.D., Department of Biomedical Engineering, Case Western Reserve University, 10900 Euclid Ave. Cleveland, OH 44106-7207. Electronic mail: gsaidel@cwru.edu

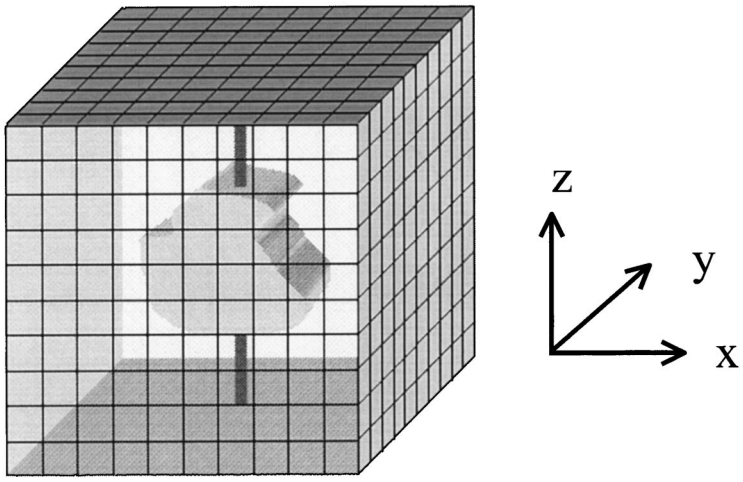

FIGURE 1. Probe along the *z* axis in the center of the *x-y* plane of a discretized cube of tissue. Tumor tissue centrally located; grid pattern illustrates the spatial discretization.

temperature image acquisition for 5 s. At the end of an ablation procedure, tissue-contrast images may be obtained to determine the extent of tumor ablation. If the tumor is not sufficiently ablated, then the rf probe is repositioned within the tumor and another ablation procedure is performed. If many model simulations could be performed within a few minutes and modified as needed by comparison to MR temperature images, then a clinician would have a better basis for predicting the effects of each step in an ablation procedure. This interactive process involving model simulation and data acquisition could be repeated for each 10 min ablation period.

Mathematical models developed to describe the tissue temperature dynamics associated with rf ablation also include a concomitant model of the electric field distributions to determine current density.[10,12,14,19] Although not usually reported, the numerical solution of these equations takes much longer than 1 min on a PC, making impractical the process of continually repeated simulations and comparison with MR images during an ablation procedure. Therefore, we present an alternative mathematical model of the tissue temperature dynamics associated with rf ablation that allows a much faster solution. This model with a heat source that decreases with distance from the rf probe obviates the need for explicit inclusion of the electric field equations. For numerical solution of the bioheat model equation, we modify and combine efficient algorithms that provide sufficiently fast simulations to be feasible for use in guiding an ablation sequence during a treatment procedure.

In the following sections, a model of 3D tissue temperature dynamics is presented. This model incorporates a heat source term based on the decreasing current flow in tissue with distance from the rf probe. Furthermore, to produce a fast numerical solution, the method of lines is applied with spatial derivatives discretized using a fourth-order approximation to produce an initial-value problem solved efficiently with a sparse-stiff integrator. From simulations of the temperature distributions of the model, the effects of thermal damage on perfusion and internal cooling of the rf probe are examined to show the versatility of the model. Then, MR temperature measurements from preliminary experiments with excised liver are shown for comparison with model simulations. Our model provides distinct advantages for analyzing the effects of rf tumor heating and ablation relative to previously published models. Finally, we discuss future quantitative validation of this modeling approach to assist in MRI guidance of tumor ablation in a clinical setting.

THERMAL MODEL DEVELOPMENT

We model the dynamic temperature distribution in a cube of tissue in which the tumor is centrally located (Fig. 1). Within the tumor, electric current from the rf probe produces a distributed heat source. The heat is dissipated by thermal conduction through the tissue and uptake by blood flowing through primarily small vessels that perfuse the tissue. We can quantify and predict the temperature distribution dynamics in tissue as a consequence of rf thermal ablation based on a local heat balance:[14,17]

$$\frac{\partial T}{\partial t} = \alpha \nabla^2 T - \omega(r,t)[T - T_b] + \sigma(r,t), \qquad (1)$$

where the temperature $T(r,t)$ is a function of r, the three-dimensional position vector, and t, time. The domain for each side of the cube is the interval $[-L,L]$. The terms on the right-hand side of Eq. (1) represent heat transfer in tissue by conduction (or thermal diffusion), the heat loss by perfusion, and the rf heat source. Since tissue thermal diffusivity α increases slightly with temperature ($<0.5\%/°C$),[6] we represent the change as a linear function:

$$\alpha(T)=\alpha_0+\alpha_1[T-T_b]. \tag{2}$$

The rate of heat loss by perfusion depends on the perfusion ω and the difference between the local tissue temperature T and blood input or (basal) temperature of tissue T_b. The perfusion function $\omega(r,t)$ varies with position and time as a consequence of reduced perfusion by blood coagulation associated with ablation. To appreciate the effect of temperature history on perfusion, we can compare the effects of two representations of the dependence of perfusion on temperature. First, consider a simple model in which perfusion exists locally in the tissue as long as the tissue temperature is below a critical value, T_C:

$$\omega(r,t)=\omega_0 U[T_C-T(0<t)], \tag{3}$$

where $U[\ ]$ is the unit step function.

Generally, the perfusion at any position and time may be described using a probability model, which reflects the local variability of the thermal response in tissue. Based on a two-state Markov process with a transition probability $\beta(t)$ between normal and thermally damaged states, the perfusion function is proportional to the probability, P_U, of no thermal damage:

$$\omega(r,t)=\omega_0 P_U=\omega_0 \exp\left[\int_0^t \beta(r,t)dt\right]. \tag{4}$$

The transition probability can be represented by Arrhenius-type activation:

$$\beta(r,t)=A\{\exp[-B/T(r,t)]\}U[T-T_0], \tag{5}$$

where A and B are constants. A tissue damage model of this character has been used by others.[12,17] With appropriate parameter values, Eq. (4) would indicate no damage even with chronic heating below a reference temperature T_0 (about 41 °C);[18] above some temperature level (about 60 °C), the rate of thermal damage is high and approaches a maximum.

The probe electrode is considered as a uniform line source located by the 3D position vector r_p (for convenience set at the x-y center along the z axis of the tissue cube from $-L_p$ to L_p). From the probe, the rf heat source $\sigma(r,t)$ is a known function of the measured input power $h_p(t)$ and varies inversely with the square of the distance from the probe, $r-r_p$:

$$r\neq r_p,\quad \sigma(r,t)=h_p(t)/[r-r_p]^2. \tag{6}$$

In other words, the source is defined only outside the domain $-L_p\leqslant z\leqslant L_p$, $x=y=0$. A formal derivation is given in Appendix A. This distance relationship for the rf heat source has been validated experimentally.[24] The probe electrode temperature variation with time is obtained independently:

$$r=r_p: T=T_p(t). \tag{7}$$

In other words, the temperature is specified only in the domain $-L_p\leqslant z\leqslant L_p$, $x=y=0$. Initially, the tissue is assumed to be at a known basal temperature:

$$t=0:\ \ T=T_0(r). \tag{8}$$

With a step input of rf power, we can simulate the probe temperature change with the approximation:

$$T_p(t)=T_b+T_\Delta[1-\exp(-t/\tau)], \tag{9}$$

where τ is a characteristic response time. Since the boundaries of the cube surrounding the tumor are far enough from the heat source, the temperature remains at the basal level:

$$r=r_\infty:\ \ T=T_b. \tag{10}$$

In other words, this condition applies when x, y, or z has the values L or $-L$.

An analytical solution of a special case of this model (Appendix B) is used for validation of the numerical solution.

NUMERICAL METHODS

For numerical solution, our objective is to implement a method that is sufficiently fast to simulate temperature distributions assuming alternative power inputs and positions of the rf electrode. To aid in decision making during MRI-guided treatment, the model must be able to predict the tissue temperature distributions for various tumor ablation strategies. A necessary tradeoff for shorter simulation times is reduced spatial resolution. Furthermore, for low cost application in the clinical setting, the computation can be accomplished on a personal computer (PC) whose speed and memory are sufficient, such as the one used for this study (600 MHz processor, 512 Mbytes of RAM). Our strategy in developing a suitable method for simulations is to use state-of-the-art algorithms that are robust, well tested, and easily implemented. For a geometrically simple system (e.g., tissue cube), we apply the method of lines or semidiscretization.[9]

In this case, the spatial derivatives of the model are represented in Cartesian coordinates. By discretizing the spatial derivatives of the model with the boundary con-

ditions incorporated, we convert the model from a parabolic differential equation into a set of differential-difference equations that constitute an initial-value problem. Each equation represents the temperature at a specific spatial node. The spatial discretization is accomplished based on a 3D extension of an efficient 1D code with fourth-order accuracy (DSS044)[16] available from the Internet (http://www.lehigh.edu/~wes1/wes1.html). The resulting initial-value problem is integrated using LSODES,[8] an efficient code for stiff and sparse systems available from the Internet (http://www.netlib.org/cgi-bin/search.pl). A Lahey PC FORTRAN compiler was used to execute these codes.

To test the accuracy of our program, we compared the method of lines solution with the numerical evaluation of an analytical solution of a special case of the bioheat transfer model (Appendix B). The analytical solution was evaluated using MATLAB (Mathworks). Summations were truncated when the difference between successive summations was less than 1%. For the $(11)^3$ node system, the numerical solution agrees with the analytical solution within 3% near the boundaries and 0.1% elsewhere. The $(21)^3$ node system increases the accuracy, reducing the error to 0.4% near the boundaries and 0.02% everywhere else. The simulation with the $(11)^3$ node system required ~12 s to reach 95% of steady state, while the simulation with the $(21)^3$ node system required ~49 min to reach 95% of steady state. Since the accuracy associated with the smaller number of nodes is sufficient for clinical application and the computational time is much less, we used this discretization for almost all simulations.

MR MEASUREMENTS

For preliminary comparison with model simulations, we obtained MR temperature data from an excised normal bovine liver. Ablation experiments were performed with a liver, refrigerated overnight, placed in a 0.2 T resistive MR imager (Magnetom Open, Siemens Medical Systems). A copper probe with a 2 cm exposed electrode coupled to a rf ablation generator (No. RFG-3C, Radionics) was inserted into the liver. To complete the circuit, a ground pad (84 cm^2) was placed under the liver providing a return path for the current. Using an echo-shifted, gradient recalled echo (ES-GRE) sequence (5 s acquisition time), phase images that produce relative temperature fields were acquired at 15 s intervals.

All images were taken perpendicular to the rf probe to easily examine deviations from symmetry. Before creating a lesion, a reference phase image at a known temperature was obtained for calibration of the experimental MR phase images with measured tissue temperature. The tissue was heated for 600 s to a steady state by maintaining the probe tip at approximately 90 °C. A thermistor located at the tip of the probe measured the temperature at the probe–tissue interface. Temperature maps were then calculated form the difference between the reference and the experimental phase images.[5] This MR thermometry technique has an accuracy of ±2 °C.

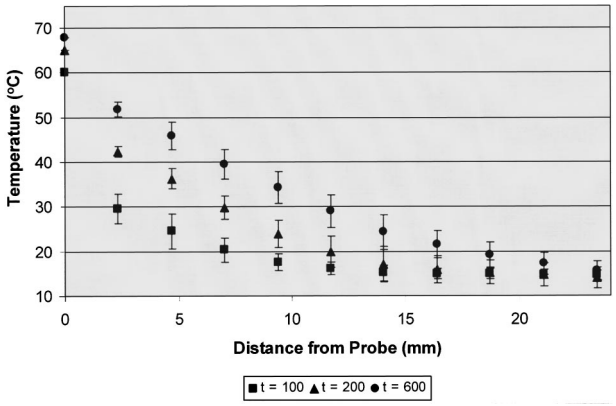

FIGURE 2. Mean spatial temperature distribution of eight equal radial distances as measured by MRI thermometry in an excised bovine liver during an ablation procedure. Three time points are shown: 100, 200, and 600 s.

From a susceptibility artifact, the probe location was determined and calibrated by the thermistor. The temperature data was filtered spatially (using a 3×3 smoothing filter) and temporally (using a three-point moving average filter) to reduce noise. Steady state temperatures were approached within 250 s after heating began. The temperature decreases rapidly with distance from the probe heat source (Fig. 2).

MODEL SIMULATIONS

Simulation Strategy

Through model simulations we can examine the effects of perfusion, ω, heat input rate, h_p, rf probe temperature, T_p, and temperature dependence of thermal diffusivity, α, on the temperature distribution in tissue. A key objective is to find a simulation strategy for increasing heat transfer from the rf electrode to the tissue periphery in order to increase the potential size of the ablated tissue (lesion). To account for a decrease in heat loss with ablation, we consider perfusion to depend on local tissue damage based on local temperature history. As described in the earlier section on model development, we present two models for the change of local perfusion with temperature. The simpler model assumes that local perfusion is eliminated when the tissue temperature reaches a threshold critical value, T_c. With the more general model, tissue damage reduces local perfusion according to the local temperature history and an Arrhenius activation function.[12,17] An issue to be addressed is the tradeoff between the generality of the perfusion modeling and the simulation speed.

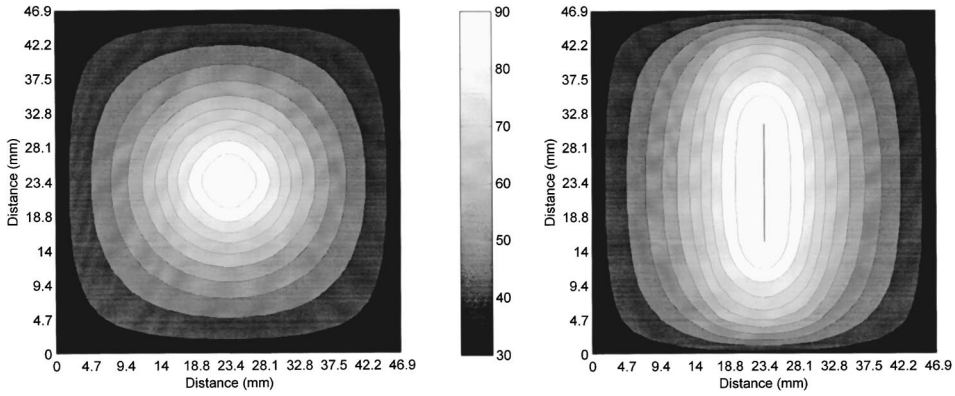

FIGURE 3. Simulated tissue temperature distribution after 600 s of heating with no perfusion and constant thermal diffusivity. $T_b = 37\,°C$, $T_p = 90\,°C$, $h_p = 4.0$, $\tau = 20$, FOV = 46.8 mm^3. Nodes: 11^3, CPU processing time: 20 s: (a) Plane perpendicular to probe in the *x-y* plane. (b) Plane along the length of probe in the *z-x* plane.

Another important aspect of model simulation is determining the maximum heat input. If the heat input rate is too great, then the tissue temperature can rise above 100 °C causing vaporization and carbonization.[7] In this case, the rate of heat transfer in tissue would decrease and the lesion size would not reach its potential. By setting the power input so that the maximum tissue temperature is no more than 90 °C, an accidental increase to the vaporization point can be avoided. With a rf probe that is not internally cooled, the maximum temperature occurs in tissue adjacent to the probe where the current density is highest. However, if the rf probe is internally cooled, then the maximum temperature will occur in tissue at some distance from the probe.[1] In this case, the heat input rate $h_p(t)$ can be increased while keeping the tissue within the maximum temperature constraint. Effectively, the temperature of the internally cooled rf probe can be decoupled from the heat input. This situation is simulated by making the step difference in temperature (T_Δ) negative so that the steady-state probe temperature ($T_b + T_\Delta$) becomes significantly lower than the surrounding tissue temperature.

Simulation Parameters

Parameter values used for the model simulations were derived from various sources. Thermal diffusivity ($\alpha = 0.15\,\text{mm}^2/\text{s}$) was based on measurements in human liver tissue as published in previous literature.[6] The basal perfusion, ω, was calculated based on a perfusion rate of 42 mL/(100 g min). For comparison with experimental data, the input power, $h_p(t)$, was calculated from experimental data and Eq. (A3) in Appendix A. For simulation with the standard probe, $h_p = 4.0$ with an average current input of 400 mA; for simulation with the internally cooled probe, $h_p = 9.0$ for which the tissue temperature did not exceed 90 °C. In the absence of specific experimental data, the probe temperature, T_p, was modeled as an exponential function with a 20 s time constant (τ) and a steady-state maximum of 90 °C. For the internally cooled probe, $T_p = 20\,°C$ in the steady state. For simulations of *in vivo* tissue, the basal tissue temperature was $T_b = 37\,°C$. The field of view (domain of the simulation) was 46.8 mm in each direction, which provides consistency between experimental data and simulations. For the threshold perfusion model, $T_C = 60\,°C$. Parameters of the Arrhenius equation, A and B, were estimated[12] to be $2.9e37$ and $3e4$.

Temperature Distributions and Transient Responses

As a reference simulation, we consider the simple case of ablating nonperfused tissue with constant properties. In the plane perpendicular to a centrally located probe, the temperature distribution is circularly symmetric about the probe when tissue properties are homogeneous and isotropic [Fig. 3(a)]. With only a few temperature nodes, especially in the neighborhood of the origin, isotherms appear noncircular as a consequence of interpolation by simple contour algorithm (contourf.m, MATLAB, MathWorks). To minimize this artifact, we applied a two-dimensional bicubic interpolation of the simulation results (interp2.m, MATLAB, MathWorks). When the probe lies in the plane of a temperature map, the temperature distribution reflects the longitudinal shape associated with the probe electrode that occupies the central node points [Fig. 3(b)]. The simulation results can also be displayed in terms of the temporal response of the tissue temperature to the rf heating at specific distances from probe (Fig. 4). With increasing distance from the probe, the response time is longer and the steady-state temperature is lower. Although not shown, the temperature dependence of thermal diffusivity has only a slight effect on the temperature distribution.

Simulations based on a threshold and temperature history models can be compared to the simulation with

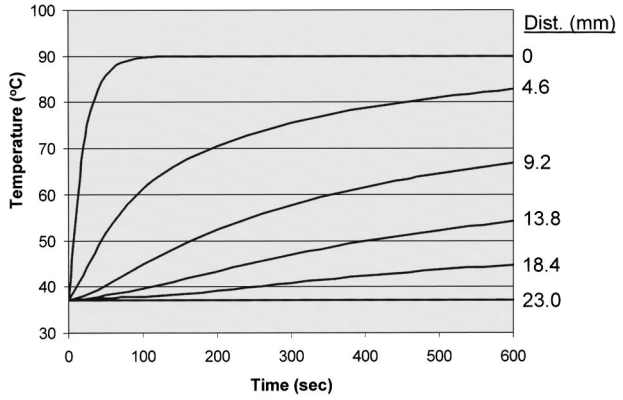

FIGURE 4. Simulated tissue temperature dynamics at several distances from the rf probe with no perfusion and variable thermal diffusivity. T_b=37 °C, T_p=90 °C, h_p=4.0, τ=20, FOV=46.8 mm^3. Nodes: 11^3; CPU processing time: 19 s.

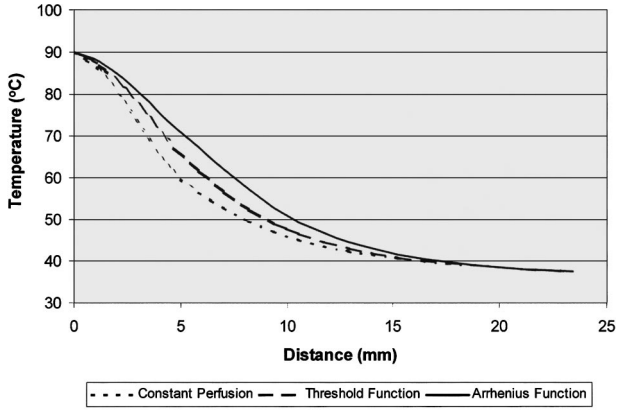

FIGURE 6. Simulated tissue temperature distribution after 600 s of heating with various perfusion expressions and variable thermal diffusivity. T_b=37 °C, T_p=90 °C, h_p=4.0, τ=20, FOV=46.8 mm^3. Nodes: 11^3. (a) Constant perfusion, CPU processing time: 19 s. (b) Constant perfusion until threshold (T_C=60 °C), CPU processing time: 60 s; (c) general perfusion model with Arrhenius equation (A=2.9e37,B=3e4). CPU processing time: 119 s.

constant perfusion (Fig. 5). At a fixed distance (4.6 mm) from the probe, the constant perfusion model reaches a steady-state temperature of 62 °C. Because of the decreased perfusion of the corresponding threshold model, a sharp change in temperature slope occurs at T_c =60 °C and the tissue temperature reaches 69 °C. With the more general model (incorporating an Arrhenius activation function), more tissue damage appears to produce a further decrease in local perfusion, which allows the temperature to reach 73 °C. A reduction in perfusion leads to less heat loss and higher tissue temperatures. From the same simulations, Fig. 6 shows the spatial temperature distribution of following 600 s of heating. These temperature distributions show that the loss of perfusion by tissue damage allows the higher temperatures to be distributed further from the probe. The greatest spread of higher temperatures is produced by the more general model.

We also simulated the tissue temperature response with an internally cooled probe that keeps the electrode temperature at 20 °C. This allows an increased heat input rate while not exceeding a tissue temperature of 90 °C, thereby avoiding vaporization. Figure 7 compares temperature distributions for the internally cooled probe (with and without perfusion reduction) and for the standard probe (without perfusion reduction). The increased

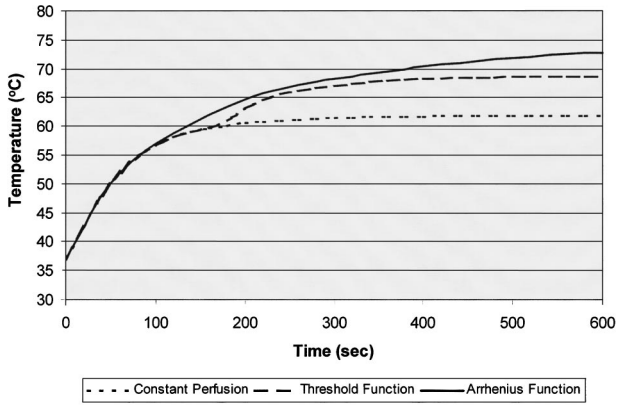

FIGURE 5. Simulated tissue temperature dynamics at one location (4.6 mm from probe) with variable thermal diffusivity and different perfusion models. T_b=37 °C, T_p=90 °C, h_p =4.0, τ=20, FOV=46.8 mm^3; Nodes: 11^3. Temperature history for simulations with (a) constant perfusion; (b) constant perfusion until threshold; and (c) general perfusion model with Arrhenius function.

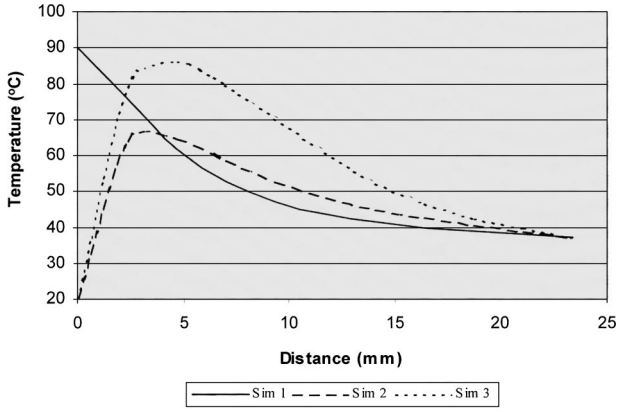

FIGURE 7. Simulations after 600 s of heating. Parameters: α=0.15, ω=0.007, T_b=37.0, τ=20, FOV=46.8 mm^3, variable diffusivity. Sim 1 assumes a standard probe with constant perfusion: h_p=4.0, T_p=90.0; Sim 2 assumes an internally cooled probe with constant perfusion: h_p=9.0, T_p=20.0, CPU processing time: 22 s. Sim 3 assumes an internally cooled probe with the Arrhenius perfusion model: h_p=9.0, T_p=20.0, A=2.9e37, B=2.44e5/8.134.

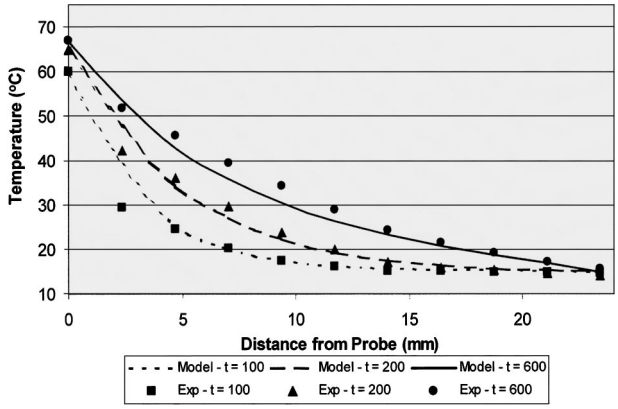

FIGURE 8. Comparison of model simulated temperature distributed at several times corresponding to experimental temperature data (using MRI thermometry) from excised bovine liver heated with a rf probe. Simulation parameters: $T_b = 15\,°C$, $T_p = 68\,°C$, $h_p = 2.7$, $\tau = 33$, $\alpha = 0.18$, FOV = 46.8 mm^3; Nodes: 11^3.

heat input rate causes higher temperatures that are distributed further from the probe. This effect is enhanced further by perfusion reduction.

As a first step in model validation, we compare the model corresponding simulation with preliminary data from excised tissue (Fig. 2) in which no perfusion occurs. In this case, we used the independently measured current input and the probe temperature that vary with time. Also, we assumed the value of thermal diffusivity given in the literature. Consequently, there are no unknown parameters in this simple case. As shown in Fig. 8, the model simulation of the temperature distribution at several times agrees well with the corresponding experimental data obtained by MRI thermometry.

DISCUSSION

Modeling Concepts

The thermal model presented here describes the 3D temperature dynamics in tissue heated by a rf heat source. The parameter values used in model simulations (given in the figure captions) were based on estimates from the literature as well as comparison with experimental data. This model is intended to allow fast, repeated simulations for clinical guidance during a rf ablation procedure with MR imaging. In the region where the temperature ranges from 41 to 60 °C, model simulation is especially important for prediction of thermal damage because of the continuously changing perfusion according to the temperature history. Local tissue temperature above 60 °C is expected to produce cell death within seconds.

A feature of this model is a heat source that decreases with square of distance from the rf probe. Such a heat source, which obviates the need for explicit inclusion electric field equations, allows much faster simulation. The source term is an approximation that assumes uniform current along the rf electrode and electrical conductivity is independent of temperature (Appendix B). Any nonuniformity would be expected to decrease with distance from the electrode. If quantitative analysis by comparison of model output with experimental data from excised tissue indicates that nonuniformities affect the source term, then the source term can be readily modified to take these into account. Each added features, however, must be balanced against the associated additional computational time for simulation.

Model Simulations

By comparison of a model simulation for a special case with an analytical solution (Appendix A), we determined the accuracy of the numerical solution. With just 11^3 nodes, the simulations of temperature distribution for the different perfusion models are sufficiently accurate for comparison with experimental data. The computation time varies from 10 s to 2 min using a PC. No other models that deal with rf ablation[10,12,14,19] can be solved numerically with such speed. In fact, for a model that includes equations for blood flow, the reported time for one simulation was 10.3 h.[10] Although this simulation time may be reduced by an order of magnitude with current computers, it would still be much too slow for use in guiding a clinical rf ablation. Although errors of a few percent occur in a region near the rf probe where the temperature gradient is large, the practical effect of this temperature inaccuracy is not expected to be significant. In this region, the temperature is high enough to ensure that ablation occurs. When we compared model simulations with 11^3 and 21^3 nodes, the accuracy of the latter is much greater, but the computational time increases by two orders of magnitude. This longer simulation time, however, makes the simulation with more nodes unfeasible for repeated application during the process of MR-guided tumor ablation.

With an internally cooled rf probe, simulation of the tissue temperature distribution was accomplished with about the same speed as that without internal cooling. Compared with other models that incorporate cooling,[1] our model does not need to describe the details of the heat transfer within the probe because the model uses the measured temperature at the probe surface as a boundary condition. Also, our model simulates 3D temperature distribution dynamics without assuming symmetry to reduce the problem to two spatial dimensions as reported previously.[17] Such symmetry is not valid when the probe is repositioned in a tumor for sequential ablations or when the tissue perfusion is not homogeneous.

During the ablation process, tissue perfusion is reduced by thermal damage. We simulated this reduction

by either a temperature threshold function or by a tissue damage function based on local tissue temperature history and incorporating an Arrhenius activation function. This latter approach is similar to that of Schwarzmaier *et al.*[17] who modeled laser-induced tumor ablation in brain tissue. In addition to the differences in application, the intention of their model was to assist in pretreatment planning rather than for guidance during ablation treatment as is the intention with our model; consequently, the numerical algorithm used by Schwarzmaier *et al.*[17] to solve their model is not particularly fast. With our model, even with the perfusion dependence on temperature history, the simulation was accomplished in about 1–2 min. This is not as fast as needed for many repeated simulations in a 10 min ablation procedure. However, several modifications to the solution algorithms could improve the efficiency of the computations. These include using a different coordinate system, adaptively grid spacing, and adaptive switching between stiff and nonstiff techniques to solve the initial-value problem. Also, computational time for simulation will continue to decrease as PC speed continues to increase significantly.

Model Validation and Implementation

Our preliminary study shows that the model simulations have characteristic behavior similar to that shown with experimental tissue temperature distributions acquired using MR thermometry. Although current MR temperature data are not as accurate as desired for quantitative comparison of the model and optimal estimation of model parameters, recent studies indicate that such data will be available soon.[2] When quantitative comparison becomes possible, then the few unknown model parameters can be estimated repeatedly for each ablation component in a clinical procedure. With this information, a clinician can examine scenarios with various probe positions and power inputs as part of a MRI-guided ablation procedure.[23] Although tissue properties have some inhomogeneity, these produce only minor effects on current heating by a 500 kHz rf power source. From this power source, the wavelength is large relative to the dimensions of both the probe and region to be ablated so that the dielectric properties of tissues can be neglected.[4]

The quantitative validation of our models require comparison of the model outputs to experimental data. Model parameters can be evaluated based on nonlinear, least-squares fitting of the predicted temperature distribution dynamics to the measured MR temperature images. At several levels of input power, the dynamic spatial distributions of the tissue temperature field from MR images can be compared with the corresponding bioheat model prediction to obtain optimal estimates of the unknown parameters and coefficients.

Further experiments with excised tissue and initial intact animal models can be used to test the mathematical model validity. As shown with the preliminary bovine liver experiment described above, excised tissue can provide a basis for experimental and model comparison. This experiment eliminates the perfusion term as well as imaging difficulties such as respiratory motion. Excised tissue experiments can also be compared with the same tissues in intact animals to validate the model representation of the perfusion dependence on temperature history. With a validated model, simulations of various power input options for each ablation step with sequential repositioning of the rf probe could be used as part of the decision-making process during an ablation treatment. Such repositioning is essential to obtain thermal lesions that conform to the shape of the tumor.

Many improvements are needed to bring this approach into clinical practice. To reduce the simulation time, improvements are needed in the numerical solution as mentioned above. In some cases, a greater spatial resolution may be needed even though a fourth-order spatial discretization is applied. Also, iterative adaptation of the thermal model during a clinical ablation procedure requires comparison of the simulations to tissue temperature dynamics obtained by noninvasive MR thermometry. This information would be integrated with MR anatomical (tissue-contrast) images and interpreted to give information about optimum sequence of rf probe orientations and power inputs to maximize tumor ablation with minimal damage to normal tissue.

The key for a model to be useful in MRI guided treatment is that the model be continually updated during the treatment process based on the MRI data obtained as the experiment progresses. In our case, we will be reestimating model parameters, especially associated with changes in the perfusion distribution, by comparing model predicted temperature distributions with MRI data. This adaptive, iterative process has not been applied previously to tumor ablation treatment with MRI guidance. Only by virtue of fast model simulations in the order of seconds is this iterative process feasible. The iterative process can be considered as a combination of feed forward by model predictions and feedback from experimental data for reestimation of model parameters. Furthermore, model simulations can yield the optimal duration for heating to produce the desired thermal damage for tumor ablation.

CONCLUSION

Our study demonstrates the feasibility of using repeated model simulations of tissue temperature dynamics interactively with MR temperature and anatomical tissue-contrast imaging to help guide the process of tumor ablation. This would lead to better prediction of the effects

of each step in an ablation procedure so that an efficient, time-saving strategy could be determined. Consequently, the potential exists for a clinician to improve the effectiveness and reliability of an interventional tumor ablation treatment.

ACKNOWLEDGMENTS

The authors would like to thank A. C. Hindmarsh and W. E. Schiesser for their generous help with the numerical solution and D. Wilson, J. Duerk, J. Lewin, and R. Brown for their assistance and helpful suggestions. This work was supported in part by the Whitaker Foundation, Siemens Medical Systems, and NIH Grant No. CA84433.

APPENDIX A

Heat Source from rf Current

The rf-generated heat term is derived from the current density and the tissue properties as follows:[3]

$$\sigma(r,t)=\frac{J^2}{k_e\rho C_P}, \tag{A1}$$

where J is the current density ($\mathrm{A\,m^{-2}}$), k_e is the electrical conductivity of tissue ($\Omega^{-1}\,\mathrm{m^{-1}}$), ρ is the density of tissue ($\mathrm{kg\,m^3}$), and C_p is the specific heat of tissue ($\mathrm{J\,kg^{-1}\,m^{-1}}$). For the case where the probe is constrained to a line source and the current is assumed to be a uniform average along the probe, the current density at any spatial location can be derived using conservation of charge. The current density is defined by

$$J=\frac{I(t)}{2\pi(r-r_p)L}, \tag{A2}$$

where I is the current (A), L is the length of the probe (m), and $r-r_p$ is the radial distance from the probe (m). Substituting Eq. (A2) into Eq. (A1) yields

$$\sigma(r,t)=\frac{I(t)^2}{(2\pi L)^2 k_e\rho C_p}\Big/(r-r_p)^2=h_p(t)/(r-r_p)^2. \tag{A3}$$

APPENDIX B

Validation of Model using Analytical Solution

To obtain an analytical solution corresponding to Eq. (1) and its initial and boundary conditions, we simplify the problem assuming a constant heat source and defining a scaled temperature $\varphi=T-T_b$ so that the boundary conditions become homogeneous:

$$\frac{\partial\varphi}{\partial t}=\alpha\left(\frac{d^2\varphi}{dx^2}+\frac{d^2\varphi}{dy^2}+\frac{d^2\varphi}{dz^2}\right)-\omega\varphi+\sigma, \tag{B1}$$

with the initial condition:

$$\varphi=0,\ \ t=0$$

and boundary conditions:

$$\varphi=0,\ \ x=0,a;\ \ y=0,b;\ \ z=0,c.$$

We solved this problem using the finite Fourier sine transform:[21]

$$\Phi_{p,q,r}(t)=\int_0^a\int_0^b\int_0^c\varphi(x,y,z,t)\sin\left(\frac{p\pi x}{a}\right)\times\sin\left(\frac{p\pi y}{b}\right)\sin\left(\frac{r\pi z}{c}\right)dxdydz. \tag{B2}$$

Applying the transform results in the following initial-value problem:

$$\frac{\partial\Phi}{\partial t}=k\Phi+B\sigma \tag{B3}$$

with the initial condition:

$$\Phi=0,t=0$$

where

$$k=A+\omega,\ \ A=-\alpha\pi^2\left[\left(\frac{p}{a}\right)^2+\left(\frac{q}{b}\right)^2+\left(\frac{r}{c}\right)^2\right],$$

$$B[1-(-1)^p]\left(\frac{a}{p\pi}\right)[1-(-1)^q]\left(\frac{b}{q\pi}\right)[1-(-1)^r]\left(\frac{c}{r\pi}\right),$$

the solution of which is

$$\Phi_{p,q,r}(t)=\frac{B\sigma}{k}[\exp(kt)-1]. \tag{B4}$$

Using the inverse transform

$$\varphi(x,y,z,t)=\left(\frac{8}{abc}\right)\sum_{p=1}^{\infty}\sum_{q=1}^{\infty}\sum_{r=1}^{\infty}\Phi_{p,q,r}(t)\times\sin\left(\frac{p\pi x}{a}\right)\sin\left(\frac{q\pi y}{b}\right)\sin\left(\frac{r\pi z}{c}\right), \tag{B5}$$

and substituting $\phi=T-T_b$, we obtain the analytical solution for T.

REFERENCES

[1] Anderson, G., X. Ye, K. Henle, Z. B. Yang, and G. Y. Li. A numerical study of rapid heating for high-temperature radiofrequency hyperthermia. *Int. J. Bio-Med. Comput.* 35:297–307, 1994.

[2] Barkauskas, K., M. Wendt, J. Lewin, and J. Duerk. PRF shift thermometry at 0.2T: A new background phase variation suppression scheme and its impact on thermal lesion fidelity. *Proc. Int. Soc. Magn. Reson. Med.* 2196, 2001.

[3] Bird, R. B., W. E. Stewart, and E. N. Lightfoot. Transport Phenomena. New York: Wiley, 1960.

[4] Cheng, Y. C., R. W. Brown, Y. C. Chung, J. L. Duerk, H. Fujita, J. S. Lewin, D. E. Schuele, and S. Shvartsman. Calculated rf electric field and temperature distributions in rf thermal ablation: Comparison with gel experiments and liver imaging. *J. Magn. Reson. Imaging* 8:70–76, 1998.

[5] Chung, Y. C., A. Shankaranarayanan, M. Hampke, E. M. Merkle, and J. S. Lewin. Temperature measurement using echo-shifted FLASH at low field for interventional MRI. *J. Magn. Reson. Imaging* 9:138–145, 1999.

[6] Duck, F. A. Physical Properties of Tissues: A Comprehensive Reference Book. San Diego: Academic, 1990, p. 18.

[7] Goldberg, S. N., G. S. Gazelle, L. Solbiati, W. J. Rittman, and P. R. Mueller. Radio frequency tissue ablation: Increased lesion diameter with a perfusion electrode. *Acad. Radiol.* 3:636–644, 1996.

[8] Hindmarsh, A. C. ODEPACK, A Systemized Collection of Ode Solvers. Scientific Computing, edited by R. Stepleman. Amsterdam: North-Holland, 1983.

[9] Iserles, A. A First Course in the Numerical Analysis of Differential Equations. New York: Cambridge University Press, 1996.

[10] Jain, M. K. and P. D. Wolf. A three-dimensional finite element model of radiofrequency ablation with blood flow and its experimental validation. *Ann. Biomed. Eng.* 28:1075–1084, 2000.

[11] Jolesz, F. A. Commentary: MR-guided thermal ablation of brain tumors. *Am. J. Neuroradiol.* 16:49–51, 1995.

[12] Labonte, S. Numerical model for radio-frequency ablation of the endocardium and its experimental validation. *IEEE Trans. Biomed. Eng.* 41:108–115, 1994.

[13] Lewin, J. S., C. F. Connell, and J. L. Duerk. Interactive MRI-guided radiofrequency interstitial ablation of abdominal tumor: Clinical safety and feasibility. *J. Magn. Reson. Imaging* 8:40–47, 1998.

[14] Panescu, D., J. G. Whayne, S. D. Fleischman, M. S. Mirotznik, D. K. Swanson, and J. G. Webster. Three-dimensional finite element analysis of current density and temperature distributions during radio-frequency ablation. *IEEE Trans. Biomed. Eng.* 42:879–889, 1995.

[15] Roemer, R. B. Engineering aspects of hyperthermia therapy. *Annu. Rev. Biomed. Eng.* 1:347–376, 1999.

[16] Schiesser, W. E., and C. Silebi. Computational Transport Phenomena. New York: Cambridge University Press, 1997.

[17] Schwarzmaier, H.-J., I. V. Yaroslavsky, A. N. Yaroslavsky, V. Fiedler, F. Ulrich, and T. Kahn. Treatment planning for MRI-guided laser-induced interstitial thermotherapy of brain tumors: The role of blood perfusion. *JMRI* 8:121–127, 1998.

[18] Seese, T. M., H. Harasaki, G. M. Saidel, and C. R. Davies. Characterization of tissue morphology, angiogenesis, and temperature in adaptive response of muscle tissue to chronic heating. *Lab. Invest.* 78:1553–1562, 1998.

[19] Shahidi, A. V., and P. Savard. A finite element model for radio frequency ablation of the mycardium. *IEEE Trans. Biomed. Eng.* 41:963–968, 1994.

[20] Sinha, S. *et al.* Phase imaging on a 0.2 T MR scanner: Application to temperature monitoring during ablation procedures. *J. Magn. Reson. Imaging* 7:918–928, 1997.

[21] Sneddon, I. A. Fourier Transforms. New York: McGraw-Hill, 1951.

[22] Zervas, N. T., and A. Kuwayama. Pathological characteristics of experimental thermal lesions: Comparison of induction heating and radiofrequency electrocoagulation. *J. Neurosurg.* 37:418–422, 1972.

[23] Zhang, Q. *et al.* A method for simultaneous rf ablation and MR imaging. *J. Magn. Reson. Imaging* 8:110–114, 1998.

[24] Zhu, L., and L. X. Xu. Evaluation of the effectiveness of transurethral rf hyperthermia in the canine prostate. *J. Biomech. Eng.* 121:584–590, 1999.